

**NASA TECHNICAL
MEMORANDUM**

NASA TM-78899

(NASA TM-78899) VSTOL TILT NACELLE
AERODYNAMICS AND ITS RELATION TO FAN BLADE
STRESSES (NASA) 15 p HC A02/MF A01 CSCL 10A

N78-26099

Unclas
63/02 23308

NASA TM-78899

**VSTOL TILT NACELLE AERODYNAMICS AND ITS
RELATION TO FAN BLADE STRESSES**

by Robert J. Shaw and Robert C. Williams
Lewis Research Center
Cleveland, Ohio 44135

and

Joseph L. Koncsek
Boeing Military Airplane Development
Seattle, Washington 98124

TECHNICAL PAPER to be presented at the
Fourteenth Joint Propulsion Conference
cosponsored by the American Institute of
Aeronautics and Astronautics and the
Society of Automotive Engineers
Las Vegas, Nevada, July 25-27, 1978

VSTOL TILT NACELLE AERODYNAMICS AND ITS RELATION TO FAN BLADE STRESSES

Robert J. Shaw and Robert C. Williams
National Aeronautics and Space Administration
Lewis Research Center
Cleveland, Ohio 44135

and Joseph L. Koncsek
Boeing Military Airplane Development
Seattle, Washington 98124

Abstract

A scale model of a VSTOL tilt nacelle with a 0.508 m single stage fan was tested in the NASA Lewis 9x15 Low Speed Wind Tunnel to ascertain inlet aerodynamic and fan aeromechanical performance over the low speed flight envelope. Fan blade stress maxima occurred at discrete rotational speeds corresponding to integral engine order vibrations of the first flatwise bending mode. Increased fan blade stress levels coincided with internal boundary layer separation occurring but became severe only when the separation location had progressed to the entry lip region of the inlet. The inlet/fan system could operate within the low speed flight envelope without incurring fan blade stress limits although boundary layer separation did occur for certain operating conditions.

Symbols

A_{ff}	fan face annulus area, 0.160 m ² (1.72 ft ²)
A_{hl}	inlet hillite area, 0.177 m ² (1.90 ft ²)
A_{th}	inlet throat area, 0.171 m ² (1.84 ft ²)
CR	inlet area contraction ratio
d	distance normal to local inlet surface
H_{b1}	boundary layer rake height, 0.191 m (0.0626 ft)
L	inlet axial length, 0.416 m (1.36 ft)
N	fan rotational speed
P_t/P_{t_∞}	local total pressure recovery
$\bar{P}_{t2}/\bar{P}_{t_\infty}$	fan face area weighted total pressure recovery
$\left(\frac{P_{t_{max}} - P_{t_{min}}}{\bar{P}_t} \right)_2$	fan face area weighted total pressure distortion
p/P_{t_∞}	local surface static pressure ratio
R_{hl}	local hillite radius
R_{hub}	fan face hub radius, 0.118 m (0.384 ft)
R_{throat}	local throat radius
R_{tip}	fan face tip radius, 0.254 m (0.833 ft)
s	inlet surface coordinate
V_∞	free stream velocity

$\frac{W\sqrt{\theta}}{\delta A_{ff}}$	fan face specific corrected airflow
x	inlet axial coordinate
α	angle-of-attack
σ	fan blade vibratory stress
σ_{max}	maximum allowable fan blade vibratory stress 2.4x10 ⁸ N/m ² p-p (3.5x10 ⁴ lb/in. ² p-p)
ϕ	angular coordinate (counterclockwise looking downstream)

Introduction

A number of potential configurations have been advanced as candidates for the Navy Type A VSTOL aircraft. One such design is the tilt nacelle concept shown in figure 1.

In the vertical ascent or descent mode, the engine nacelles are rotated to approximately 90° with respect to the aircraft axis as shown in Fig. 1(a). The thrust from the two tilt nacelles provide two support posts for the aircraft while the third is provided by the nose fan which is driven by the tilt nacelle powerplants.

In the cruise mode the nacelles are rotated so as to roughly align with the aircraft axis as shown in Fig. 1(b). The nose fan is not employed in the cruise mode.

The inlets for the tilt nacelles will experience high angles-of-attack at the low forward velocities characteristic of the take off and landing maneuvers. Representative operating conditions as determined by mission studies for such inlets are shown in Fig. 2. It can be seen that tilt nacelle inlets can experience angles-of-attack as high as 120° at a flight velocity of 21 m/sec (40 knots). Such severe operating conditions can result in boundary-layer separation within the inlet resulting in increases in total pressure distortion presented to the powerplant. A major concern is that the internal flow separation can result in intolerable levels of fan blade vibratory stress which could in turn result in fan blade failure.

A number of experimental programs have been conducted in the past which were concerned with the aerodynamic characteristics of STOL inlets when internal flow separation occurred.¹⁻⁶ Since an inlet for a VSTOL application would in general have increased angle-of-attack requirements, the effects of internal flow separation would be expected to be more severe both on inlet performance and resultant fan blade stress levels.

In order to evaluate the aerodynamic-aeromechanical interrelationships and thus to help evaluate the viability of the tilt nacelle concept,

a joint test program was initiated between NASA Lewis Research Center and Boeing Military Airplane Development to test a scale model of a candidate tilt nacelle design with a single stage fan. The intent was to document the inlet aerodynamic and fan aeromechanical performance over the low speed operational envelope of Fig. 2. The overall results of the test program are discussed in Ref. 7. This paper will concentrate on one of the five design goal points ($V_\infty = 54$ m/sec (105 knots), $\alpha = 75^\circ$) and discuss the salient inlet aerodynamic features and the resultant fan blade vibratory stress signature. Finally the blade stress induced limits on the safe nacelle operating envelope will be discussed.

Apparatus and Procedure

Test Model

A schematic of the inlet-fan combination is shown in Fig. 3.

The inlet was designed by Boeing Military Airplane Development to be a candidate design for a tilt nacelle subsonic VSTOL aircraft. The inlet is an asymmetric design with a local contraction ratio (R_{h1}/R_{throat})² varying from 1.76 in the windward plane to 1.30 in the leeward plane. The overall inlet contraction ratio (A_{h1}/A_{throat}) is 1.50.

The intent of the design is twofold: (1) to provide a high enough contraction ratio in the windward region to minimize the static pressure gradients imposed on the internal boundary layer and, hopefully, inhibit boundary layer separation and (2) to keep the overall inlet contraction ratio low enough to delay the drag rise Mach number to a sufficiently high value. A further discussion of the inlet design philosophy is given in Ref. 8.

The fan is a single stage 0.508 m diameter design which has a pressure ratio and tip speed representative of the Type A VSTOL aircraft application. At the nominal design speed of 8020 rpm, the fan pressure ratio is approximately 1.17 and the tip speed is 213.5 m/sec. At the maximum fan speed of 120 percent of the design value, the fan pressure ratio is 1.25 and the tip speed is 256 m/sec.

The fan has 15 rotor blades and 25 stator blades with a rotor-stator spacing of approximately one rotor tip chord length. The rotor blades were fabricated from a titanium alloy and have circular arc airfoil sections.

The fan has provisions for adjusting the blade pitch and hence has no midspan dampers. All test runs were conducted with the blades set at the design angle.

The fan is driven by a four-stage turbine powered by high pressure, heated air delivered to the turbine through flow passages in the model support strut.

The fan nozzle exit area was sized to duplicate as closely as possible the operating line used in a previous full scale inlet-engine test in the NASA Ames full scale wind tunnel.⁸

A more complete discussion of the aerodynamic characteristics of the fan can be found in Ref. 9.

Instrumentation

The model instrumentation is shown in Fig. 4.

The inlet had axial rows of static pressures located at three circumferential angles. For this discussion, only the windward plane distributions will be presented.

Two removable six tube boundary layer total pressure rakes were located about midway in the diffuser of the inlet ($X/L = 0.63$) to determine the quality of the diffuser flow. One of the rakes was located 5° from the windward plane while the second was located 50° from the windward plane.

The quality of the flow entering the fan was determined through the use of six equally spaced total pressure rakes each containing 19 total pressure probes. (One rake was located in the windward plane.) Six of the probes on each rake were positioned to provide an equal area weighted measurement of the fan face flow while the remaining tubes were positioned so as to provide a more detailed measurement of the outer surface boundary layer and mid-channel flow. The closest total pressure probe to the outer wall was located 0.6 percent of the duct height away from the wall.

Six outer surface static pressure taps were located in the fan face plane and located midway between the fan face rakes.

To detect the onset of internal flow separation within the inlet, a miniature dynamic high response total pressure transducer was mounted in the fan face rake plane 2.79 cm from the outer surface and displaced 7.5° from the windward plane. The rms output of the transducer was displayed on line during the test.

The fan blade vibratory stresses were measured using three strain gages located at the root of the suction side of the chosen blades at approximately the mid chord position. This position was responsive to all blade vibrational modes and each strain gage was calibrated in terms of the maximum stress for each mode. All three gages were monitored during the test and indicated essentially identical readings. Thus for purposes of this discussion only one of the three strain gage signals was analyzed.

Test Facility

The test discussed herein was conducted in the NASA Lewis 9x15 Low Speed Wind Tunnel which is an atmospheric total pressure facility with a free stream velocity range of 0 to 75 m/sec.

A photograph of the model installed in the test section is shown in Fig. 5. The model rotates in a horizontal plane about a vertical support post which also provides a passage for the high pressure turbine drive air. A portion of the adjacent wind tunnel vertical wall was removed to allow the fan and turbine exhaust fans to pass through the wind tunnel during the high angles of attack.

Test Procedure

A major concern during the test was the safety of the fan since it was anticipated that at the extreme operating conditions, fan blade stresses in excess of limit values could be encountered. Such a

concern dictated that the following test procedure be employed.

Initially a low free stream velocity and angle-of-attack were established with the fan operating at a low speed (~1000 rpm) which usually corresponded to separated inlet flow. The fan speed was thus increased while the stress levels were continually monitored until a speed of about 8000 rpm was reached. If at any time the fan blade stresses reached a limit value, the test sequence was immediately discontinued and the fan speed reduced to a safe condition. Such a sweep in fan speed was termed a safety sweep.

Once the safety sweep had established that fan blade stresses were not excessive, the fan speed was slowly decreased until the dynamic pressure transducer showed increased activity which was indicative of boundary layer separation. A number of steady state data points were then taken to determine the actual onset of separation through the inspection of the windward plane fan face total pressure rake profiles. Additional data points were also taken to document inlet/fan performance with increasingly severe degrees of separation as well as with an attached boundary layer flow.

At each free stream velocity the angle-of-attack was increased in increments of 15° beginning with $\alpha = 0^\circ$ and the above described process repeated until limiting values of stress or the desired angle-of-attack was reached. This process was then repeated for increased free stream velocities.

In this manner, the envelope of safe operating conditions was investigated (Fig. 2).

Results and Discussion

As already indicated, one of the five low speed design goal operating points was chosen for analysis and presentation. The results to be shown were typical of the overall test results.

Figure 6 presents the fan blade vibratory stress signature measured for $V_\infty = 54$ m/sec (105 knots), $\alpha = 75^\circ$. Also shown for comparison is the stress signature for $V_\infty = 54$ m/sec (105 knots), $\alpha = 0^\circ$.

The first, flatwise bending mode stress signature is shown as a percentage of the maximum allowable stress as a function of both inlet specific corrected airflow ($W/\delta A_{eff}$) and fan rotational speed (N). The test results indicated the only significant mode of vibration present was the first flatwise bending mode. The maximum allowable vibratory stress as determined by a combined analytical/experimental procedure was 2.4×10^8 N/m² peak-to-peak (3.5×10^4 lb/in.² p-p).

The stress signature can be characterized as having two components: a broadband level superimposed on which are a series of discrete narrow speed band peaks. These discrete narrow peaks correspond to integral numbers of blade vibration cycles per rotational cycle and hence are designated as the integral engine order vibrations (EO's). That is the engine order three (EO3) vibration corresponds to three cycles of vibration per rotational cycle.

The integral engine order vibrations always occur at the same rotational speeds, but the corresponding inlet airflow will vary with free stream velocity.

The stress signature corresponding to $\alpha = 75^\circ$ indicates that engine order three through six vibrations (EO3 through EO6) were present with the engine order five vibration (EO5) reaching approximately 80 percent of the limit value.

A comparison of the two stress signatures shown indicates the significant effect the inlet aerodynamics have on the resulting vibratory blade stress levels. The signature corresponding to $\alpha = 0^\circ$ inlet/fan operation can be characterized as a flat broadband profile with small increases in stress level corresponding to the EO3, EO4, and EO5 vibration peaks. The maximum stress level corresponds to the EO3 vibration peak and is less than 10 percent of the maximum allowable stress level. Increasing the angle-of-attack to 75° and repeating the sequence results in a significantly different stress signature. The broadband stress level is no longer flat but shows a large increase in the neighborhood of 4000 rpm. The engine order vibration peaks are also increased in level over the corresponding $\alpha = 0^\circ$ levels. In addition the relative levels of the engine order peaks are changed from the $\alpha = 0^\circ$ signature.

In order to understand the cause/effect relationship between the inlet aerodynamics and the blade stress signature already shown, the appropriate inlet aerodynamic data will be presented and discussed.

Figure 7 relates the overall inlet performance in terms of the usual inlet parameters of area weighted total pressure recovery and total pressure distortion to the stress signature for $\alpha = 75^\circ$ already shown. The recovery levels were calculated from the fan face rake measurements by taking all 19 probes into consideration. Two distortion calculations are shown - one corresponding to deleting the outer nine percent of the fan face annulus area and the other corresponding to deleting the outer 26.6 percent of the area. The filled symbols indicate that separated flow was indicated by the windward plane fan face rake profile.

The figure indicates that the inlet total pressure recovery levels are high regardless of the level of fan blade stress level encountered. The recovery is in excess of 99 percent when the boundary layer is attached and drops to only 97 percent for the lowest inlet airflow for which data were recorded.

It should be pointed out that boundary layer separation is encountered as the fan speed and hence inlet airflow level are decreased from higher to lower levels (that is, proceeding from right to left on this and subsequent figures). As might be expected as the inlet airflow is reduced and separation is detected, both of the calculated distortion parameters increase, reach a maximum value and then decrease for further reductions in inlet airflow. The maximum level of distortion can be seen to occur at approximately the same inlet airflow as does the maximum blade stress level.

The 91 percent area distortion parameter has much higher attached flow distortion levels than does the 73.4 percent area parameter. This can be

attributed to the fact that the 91 percent area parameter uses total pressure measurements which are within the attached boundary layer for the distortion level calculation. The high levels of attached flow distortion tend to mask the effect of the total pressure distortion on the blade stress signature as shown in Fig. 7. That is the distortion levels are relatively high for low stress conditions and do not increase appreciably for those conditions for which the blade stress does increase significantly. This fact was noted for all the test data analyzed.

Such an occurrence prompted the introduction of the 73.4 percent area distortion parameter which was defined to consider only those measured total pressures which are outside the attached flow boundary layer. As Fig. 7 indicates, the variation of the 73.4 percent area distortion parameter does tend to agree more with the blade stress signature in a qualitative fashion.

Figure 7 also indicates that a significant reduction in inlet airflow could be effected once separation is first observed prior to reaching the maximum vibratory stress level. This result was also observed throughout the test program.

The combination of high total pressure recovery and high distortion implies that that a small region of locally low recovery exist at the fan face. This will be illustrated in the following figure.

Figure 8 relates the inlet aerodynamic characteristics to the fan blade vibratory stress characteristics for a series of inlet airflows. For each airflow, the figure shows the stress signature already discussed, the fan face total pressure contour map, the appropriate individual fan face rake profiles, and the two mid-diffuser boundary layer rake profiles. Figure 9 presents the windward surface static pressure distributions for the same airflows.

For the high inlet airflow (168 kg/sec-m^2 , 34 lbm/sec-ft^2) shown in Fig. 8(a), the stress level is low (-5 percent) and the contour map indicates an asymmetric boundary layer thickness distribution, a fact substantiated by the windward and leeward fan face rake profiles shown which both show attached flow profiles. Likewise the two mid-diffuser profiles indicate an attached boundary layer flow although some profile distortion is noted for the $\phi = 5^\circ$ rake. It should be noted that the radial position scales for the boundary layer and fan face rake profiles are the same which allow a direct comparison of the profiles to be made.

It is interesting to note that while the stress level corresponding to an inlet airflow of 168 kg/sec-m^2 (34 lbm/sec-ft^2) is low, an increase in inlet airflow to that corresponding to the engine order three (EO3) vibration results in a sizable stress level (-30 percent). The EO3 vibration peak is significant even though the inlet boundary layer flow is definitely attached. It is hypothesized that an attached asymmetric boundary layer thickness distribution at the fan face like that shown in Fig. 8(a) is responsible for the increased stress level.

As the inlet airflow is reduced to 147 kg/sec-m^2 (30 lbm/sec-ft^2) as shown in Fig. 8(b), the

contour map shows little apparent variation from that of the higher airflow already shown. However, the windward plane ($\phi = 0^\circ$) fan face rake profile indicates separated flow exists at the fan face. The fully developed profile corresponding to the $\phi = 60^\circ$ rake indicates the separation is a localized phenomenon which exists over only a small sector of the fan face plane. The $\phi = 5^\circ$ mid-diffuser boundary layer rake shows a distorted although still attached profile indicating the separation location is downstream of the measurement plane. The $\phi = 50^\circ$ rake still indicates a well developed boundary layer profile.

For future reference, this condition shown in Fig. 8(b) will be termed that condition corresponding to the onset of diffuser separation and will be indicated as DS on future stress plots.

If the windward surface static pressure distributions corresponding to the two conditions already discussed are examined (Fig. 9), little if any indication of the occurrence of boundary layer separation can be detected as the profiles are qualitatively very similar in nature.

A slight reduction in inlet airflow to that level corresponding to the engine order four vibration results in a significant increase in stress level (-35 percent). Apparently the rather small zone of separated flow present is sufficient to induce an increased vibration amplitude. This is especially noticeable when the EO4 vibration level (-35 percent) is compared to the EO4 level corresponding to $\alpha = 0^\circ$ operation (-5 percent).

It is important to note that the location of the initial point of boundary layer separation is stable. That is as long as the inlet airflow is kept constant the separation does not propagate forward to the entry lip region of the inlet.

Figure 8(c) corresponds to the inlet airflow (119 kg/sec-m^2 , 24 lbm/sec-ft^2) for which the fan face distortion level was the highest measured to the free stream conditions (V_∞ , α) being discussed. The broadband stress level increased significantly over that for the two hour airflows already discussed. The contour map shows a relatively extensive spoiled sector which extends over about a 90 degree circumferential extent.

The windward plane fan face rake profile shows a large separated zone extending over about 30 percent of the duct height. The total pressure levels near the outer (tip) surface are less than the local outer surface static pressure. This could be indicative of a region of reversed flow existing with the total pressure probes essentially reading a base pressure level. The occurrence of this supposed flow reversal appears to coincide with the maximum stress levels encountered during the test (for any given V_∞ , α).

The fan face profile at $\phi = 60^\circ$ still shows an attached profile which indicates the circumferential extent of the separated zone is less than 120° ($\pm 60^\circ$).

The $\phi = 5^\circ$ mid-diffuser boundary layer rake profile indicates the location of separation was well forward of this station. The profile for $\phi = 50^\circ$ is attached although profile distortion is evident.

The corresponding windward surface static pressure distribution (Fig. 9) shows a distinct pressure plateau indicative of boundary layer separation which starts at approximately the inlet throat station. The difference in character between the pressure profile and the preceding ones is evident.

It can be hypothesized that the level of fan blade stress is mainly a function of the distortion level (an intensity) as well as the distortion pattern (an extent). The significant increase in the E05 stress level seems to agree with this hypothesis as both the distortion intensity and extent increased when compared to the data shown for the previous inlet airflows.

A further reduction in inlet airflow to 88 kg/sec-m² (18 lbm/sec-ft²) as shown in Fig. 8(d) results in a significant change in the character of the fan face total pressure contour map. No longer is the contour map essentially symmetric about the windward-leeward plane as it is for the previous conditions presented. The fan face profiles indicate the flow is separated over large portions of the fan face area. These two mid-diffuser boundary layer rake profiles show separated flow also exists at that station.

The stress level for this inlet airflow is relatively low. Even though the extent of the fan face distortion is large, the intensity has decreased. This appears to agree with the hypothesis already advanced about blade stress being a function of both the distortion level (intensity) and pattern (extent).

The windward surface static pressure distribution (Fig. 9) corresponding to this low airflow condition shows that the separation location is approximately at the hilite of the inlet. Although not shown here, the static pressure distributions corresponding to $\alpha = 45^\circ$ and 180° also indicate separated flow existed from the vicinity of the hilite - at those two circumferential positions.

The vibratory stress plot shown in Fig. 8(d) shows an inlet airflow corresponding to separation reaching the vicinity of the inlet entry lip region and designated as LS. This occurrence was determined by monitoring a windward plane surface static pressure located approximately halfway between the inlet hilite and throat locations.

The fan blade vibratory stress level reaches a maximum in broadband level when the separation location reaches the vicinity of the inlet lip. This correlation between broadband stress maxima and separation location held throughout the test matrix investigated. It should be noted that while the broadband stress maxima occur when the separation location reaches the vicinity of the inlet lip, the absolute maxima in stress occur at the fan speeds corresponding to the integral engine order vibrations.

The fact that the separation location is stable in that its location can be controlled by the amount of inlet airflow demanded by the fan suggests that two separation boundaries for the inlet are important. These two boundaries are shown in Fig. 10 as the boundary which describes the initiation of separation within the diffuser and a second boundary which indicates when the separation

reaches the vicinity of the inlet lip. It should be noted that the two boundaries shown in Fig. 10 hold only for a free stream velocity of 54 m/sec (105 knots). Different absolute boundaries would exist for each free stream velocity.

The figure indicates that a significant reduction in inlet airflow can be tolerated once diffuser separation occurs prior to the separation location reaching the vicinity of the inlet lip. It is important to restate that for the test conducted, the separation location was stable and the inlet/fan combination would be operated indefinitely in the shaded region without any uncontrolled movement of the separation location occurring.

If indeed for an actual flight application, the separation location was again stable, the operational envelope of the inlet could be significantly increased by allowing the inlet boundary layer to separate but keeping the separation location from reaching the vicinity of the inlet lip. However, it must be borne in mind that the final determination of the inlet fan operational envelope can only be made when the levels of fan blade vibratory stress encountered are known.

The fan blade vibratory stress signature discussed was generated by reducing the fan speed for a given model angle-of-attack. Such a procedure allowed the determination of the stress levels corresponding to the various integral engine order vibrations as well as any other broadband stress maxima.

It would be instructive to examine how the stress levels corresponding to the integral engine order vibrations vary with increased angle-of-attack. However, the extremely narrow widths of the integral engine order vibration peaks made such a determination difficult. For this reason, cross plots of stress level versus angle-of-attack were prepared using the more easily obtainable stress signatures already discussed.

Figure 11 shows the variation of the engine order five (E05) stress level with angle-of-attack for a free stream velocity of 54 m/sec (105 knots). Also shown are the appropriate fan face total pressure contours. It has already been shown that this stress peak was the maximum for this free stream velocity. Other test data showed that for a majority of test conditions, this stress peak was the maximum encountered.

The figure indicates that the stress level is initially low (~2-5 percent) but only increases slightly (~10 percent) when diffuser separation initially occurs ($\alpha = 60^\circ$). Further increases in model angle-of-attack result in a continuously increasing stress with a level of about 80 percent being reached at 75 degrees. The increasing vibratory stress levels correspond to the separation location moving forward in the inlet toward the entry lip region. This figure also points out the additional inlet angle-of-attack capability available if the boundary layer is allowed to separate but the separation location is kept downstream of the vicinity of the inlet lip.

As already indicated the available inlet operational envelope can only be determined once the fan blade vibratory stress characteristics are known. As noted for a majority of test conditions, the

engine order five (E05) stress peak was the maximum stress level encountered for given operating conditions (V_∞ , α).

With these thoughts in mind, the measured E05 stress levels were compared to the desired inlet low speed design goal points and the results are shown in Fig. 12. (It should be recalled that the E05 stress occurs at a fixed fan speed which corresponds to an inlet airflow which varies with free stream velocity.)

The comparison indicates that the inlet/fan system tested could operate at the design goal points without incurring limiting values of E05 stress. However, the stress levels encountered were as high as about 80 percent of the limit value. The figure indicates that the E05 stress level was the highest for the operating point ($V_\infty = 54$ m/sec, $\alpha = 75^\circ$) discussed herein.

Also shown on the figure are the two appropriate aerodynamic separation boundaries which have already been discussed. It can be seen that the onset of diffuser separation would result in E05 stress levels of 40 percent or less. This indicates that for all free stream velocities the initial diffuser separation would be localized and thus would not excite the E05 vibration to intolerable levels.

The lip separation boundary can be seen to roughly agree with a limit E05 stress contour ($\sigma/\sigma_{\max} = 100$ percent) if one were estimated from the contours which are shown. This indicates that regardless of free stream velocity, the distortion (i.e., intensity and extent) associated with the forward movement of the separation location to the vicinity of the entry lip region excites the E05 vibration to near limit levels.

Several points should be raised when this figure is examined. The aerodynamic-aeroelastic correlation holds only for the fan/inlet combination tested. Other fan designs with different aerodynamic properties, or which have blades fabricated from other materials (e.g., composites) would be expected to have significantly different vibratory stress tolerance characteristics. Also the problems of inlet aerodynamic and fan aeromechanical scaling to expected full scale performance are currently not well understood.

However the results shown herein indicate the compatibility between the inlet aerodynamic and fan blade vibratory stress characteristics will be of key concern in the design of a viable tilt nacelle VSTOL aircraft. It can also be hypothesized that other VSTOL aircraft designs (e.g., configurations employing thrust deflecting nozzles) may also experience significant vibratory stress levels.

Clearly much additional work is required to identify the proper aerodynamic descriptive parameters in order to quantify the fan blade vibratory stress compatibility problem.

Summary of Results

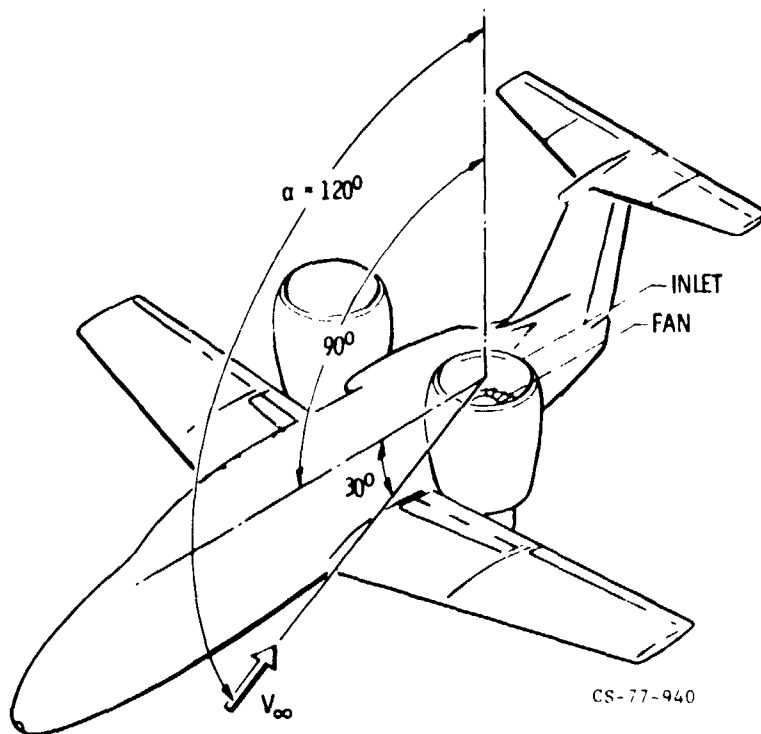
A scale model of a tilt nacelle inlet designed for the proposed Navy Type A VSTOL aircraft was tested in the NASA Lewis 9x15 Low Speed Wind Tunnel. The inlet was coupled to a 0.508 m diameter single stage fan and tested over the expected low speed flight envelope. The major results can be summarized as follows:

marized as follows:

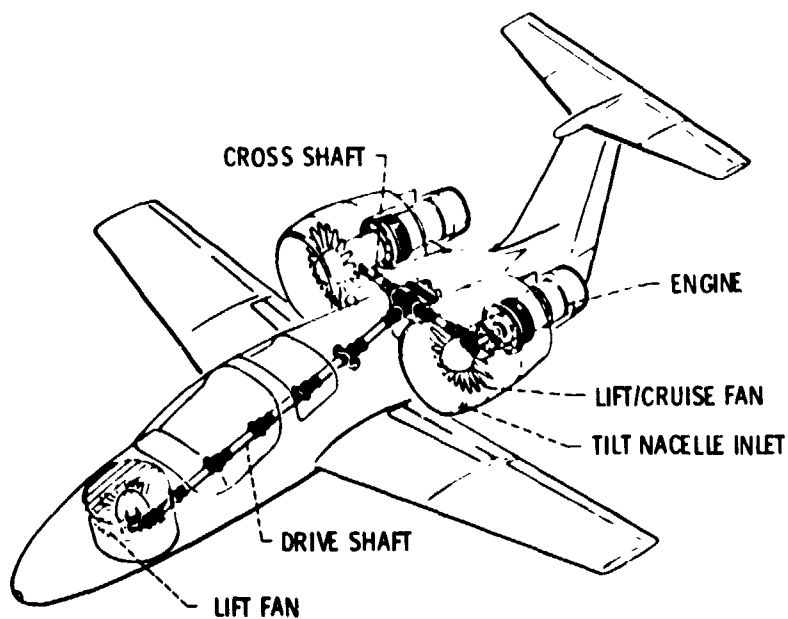
1. Significant fan blade vibratory stress levels were encountered which corresponded to integral engine order vibrations. These narrow fan speed band peaks corresponded to the first flatwise bending mode.
2. The highest levels of fan blade stress coincided with internal boundary layer separation occurring about the windward plane of the inlet.
3. Stress maxima appeared to coincide with the boundary layer separation location reaching the vicinity of the entry lip region of the inlet.
4. The internal boundary layer separation initially occurred well downstream in the diffuser and the separation location was stable. That is the separation location moved forward only as the inlet airflow demanded by the fan was decreased. A significant decrease in inlet airflow was necessary between the initial occurrence of separation in the diffuser and the separation location progressing to the entry lip region of the inlet.
5. Even though inlet separation did occur at various operating conditions within the low speed flight envelope, the inlet/fan system tested could operate over the envelope without incurring fan blade vibratory stress levels in excess of the limit value.

References

1. Jakubowski, A. K., and Luidens, R. W., "Internal Cowl Separation at High Incidence Angles," AIAA 75-64, Jan. 1975.
2. Miller, B. A., Dastoli, B. J., and Wasoky, H. L., "Effect of Entry-Lip Design on Aerodynamics and Acoustics of High Throat-Mach-Number Inlets for the Quiet, Clean, Short Haul Experimental Engine," NASA TM X-3222, 1975.
3. Miller, B. A., "Inlets for High Angles of Attack," *Journal of Aircraft*, Vol. 13, No. 4, Apr. 1976, pp. 319-320.
4. Linden, R. W., and Abbott, J. M., "Incidence Angle Bounds for Lip Flow Separation of Three 13.97 Centimeter-Diameter Inlets," NASA TM X-3351, 1976.
5. Miller, B. A., "A Novel Concept for Subsonic Inlet Boundary-Layer Control," *Journal of Aircraft*, Vol. 14, No. 4, Apr. 1977, pp. 403-404.
6. Abbott, J. M., "Aeroacoustic Performance of a Scoop Inlet," AIAA 77-1354, Oct. 1977.
7. Koncsek, J. L., and Shaw, R. J., "Operating Characteristics of an Inlet Model Tested with a 0.5 M Powered Fan at High Angles-of-Attack," Boeing Co., Seattle, Wash., D180-20798-1, Sep. 1977. (NASA CR 135270.)
8. Syberg, J., and Koncsek, J. L., "Low Speed Tests of a Fixed Geometry Inlet for a Tilt Nacelle V/STOL Airplane," Boeing Co., Seattle, Wash., D180-20276-1, Jan. 1977. (NASA CR-151922.)
9. Lewis, G. W., Jr., and Tysel, E. R., "Overall and Blade-Element Performance of a 1.20-Pressure Ratio Fan Stage at Design Blade Angle Setting," NASA TM X-3101, Sep. 1974.



(a) LANDING/TAKEOFF CONFIGURATION.



(b) CRUISE CONFIGURATION.

Figure 1. - Tilt nacelle VISTOL aircraft.

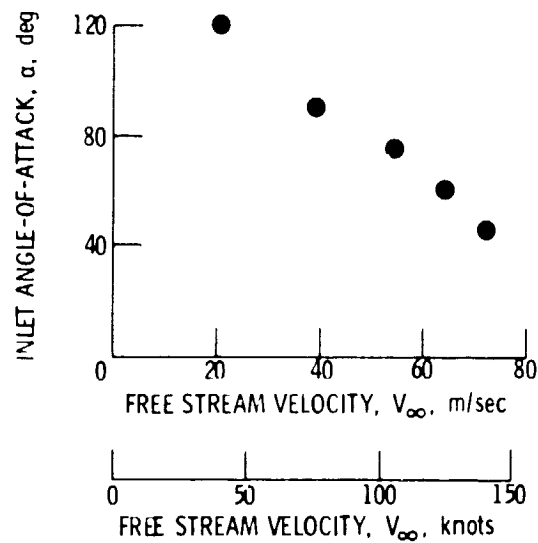


Figure 2. - Tilt nacelle inlet low speed design goals.

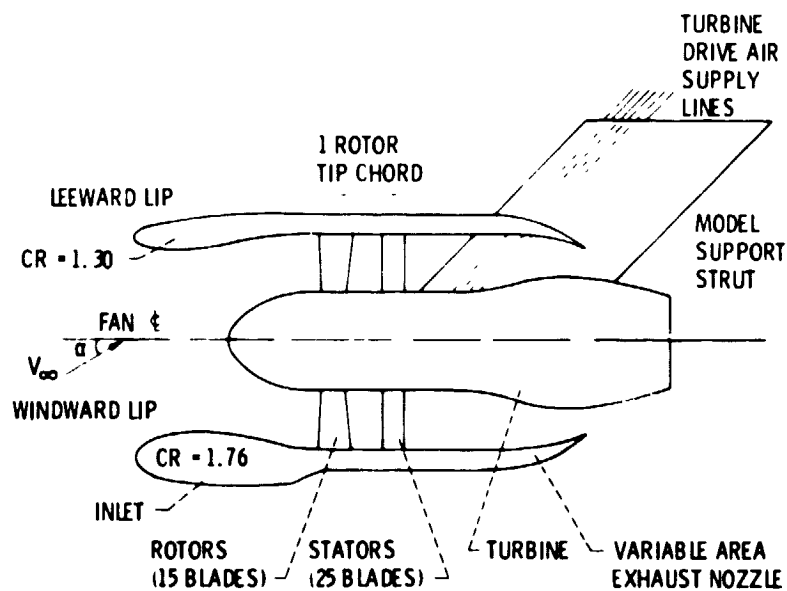


Figure 3. - Inlet/fan assembly.

ORIGINAL PAGE IS
OF POOR QUALITY

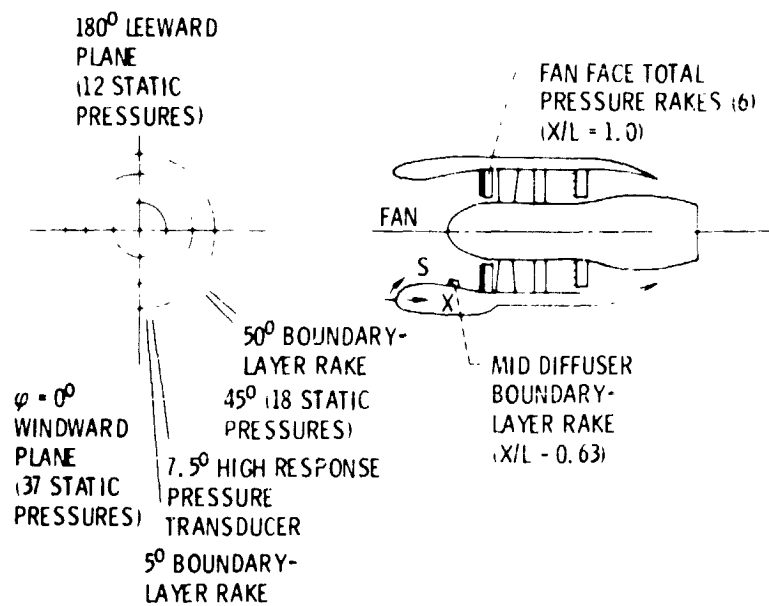
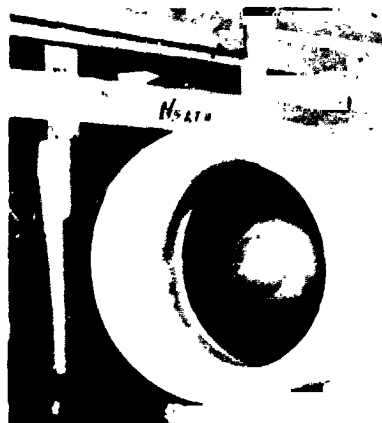


Figure 4. - Instrumentation locations.



C-77-1662

Figure 5. - Tilt nacelle inlet/fan installed in NASA-Lewis 9 X15 foot low speed wind tunnel.

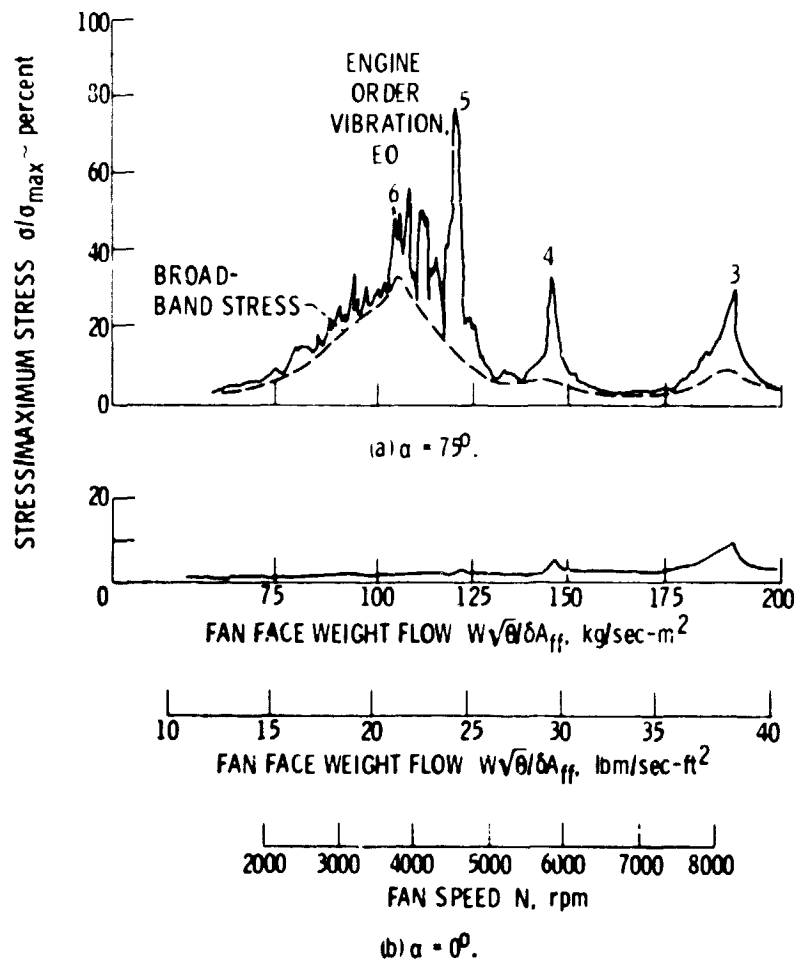


Figure 6. - Fan blade vibratory stress characteristics (first flat-wise bending mode) for $V_\infty = 54$ m/sec (105 knots).

ORIGINAL PAGE IS
OF POOR QUALITY

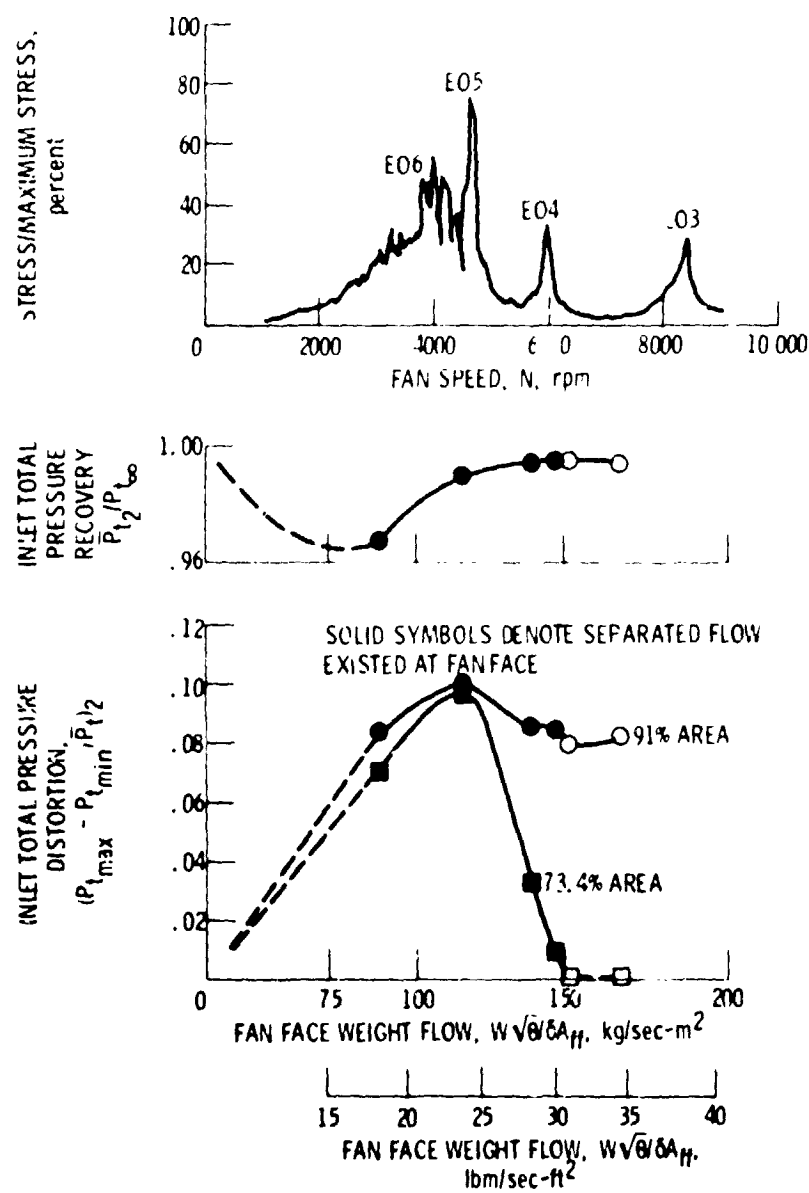


Figure 7. - Inlet aerodynamic performance and fan blade vibratory stress characteristics, $V_\infty = 54$ m/sec (105 knots), $\alpha = 75^\circ$.

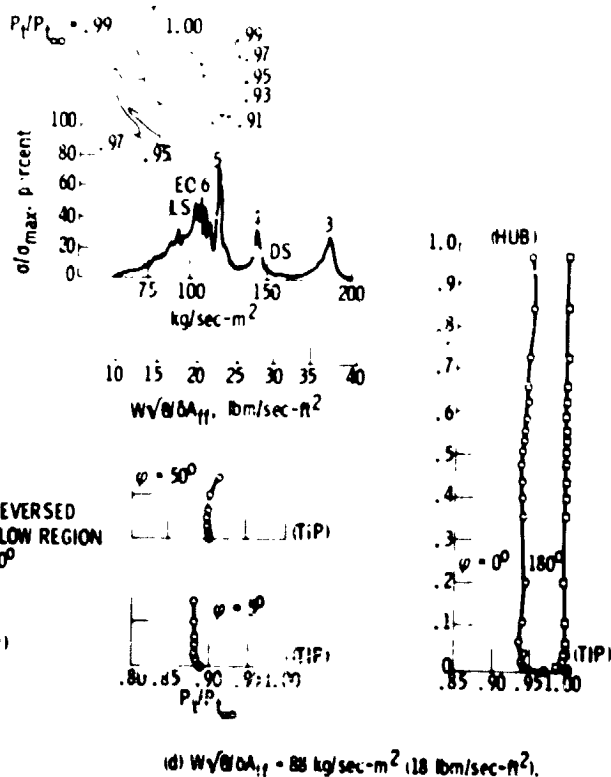
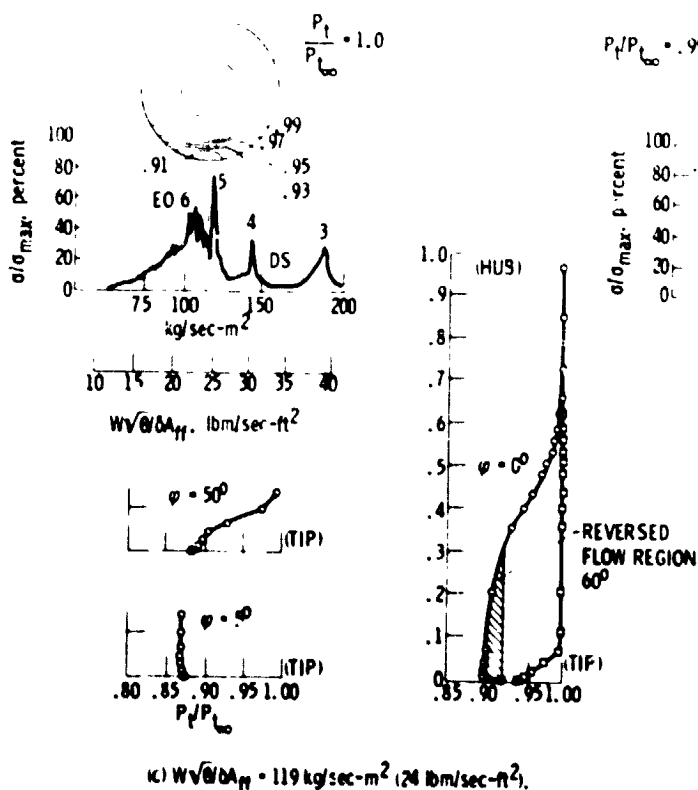
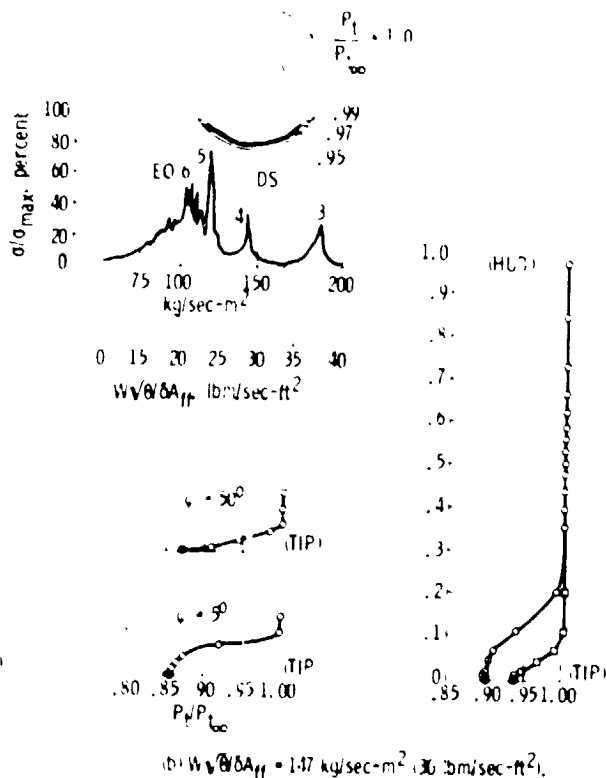
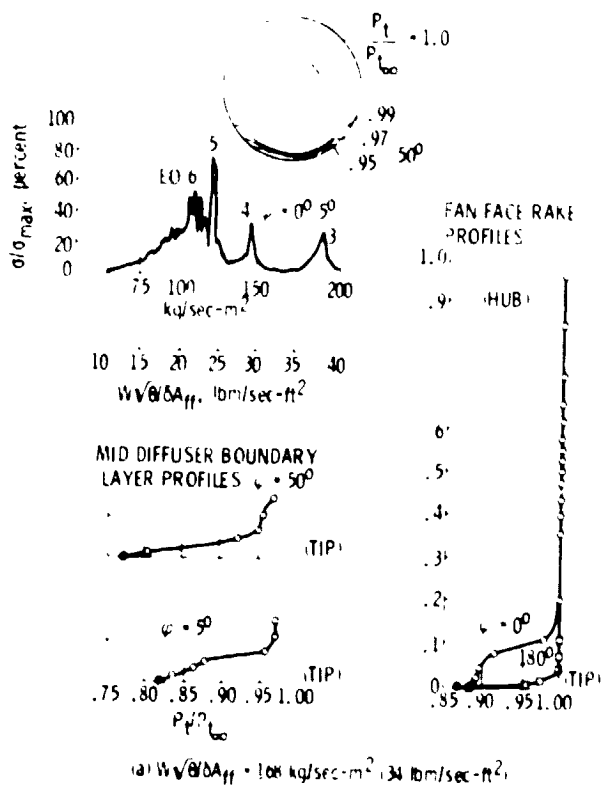


Figure 8. - Correlation of fan blade stress signature with inlet performance $V_\infty = 54 \text{ m/sec}$ (105 knots), $\alpha = 7.9^\circ$.

2-635

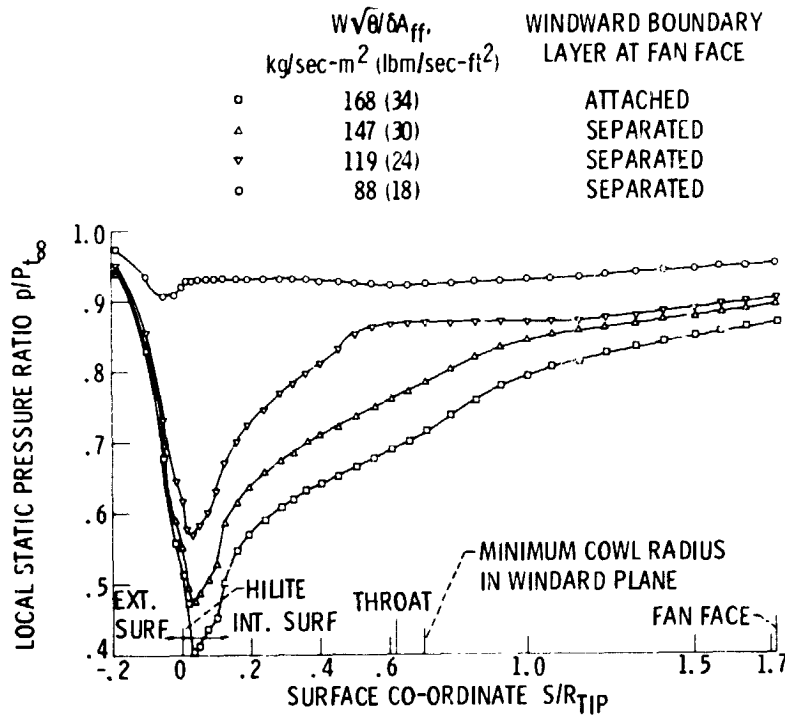


Figure 9. - Tilt nacelle inlet windward surface static pressure profiles for $V_{\infty} = 54$ m/sec (105 knots), $\alpha = 75^\circ$.

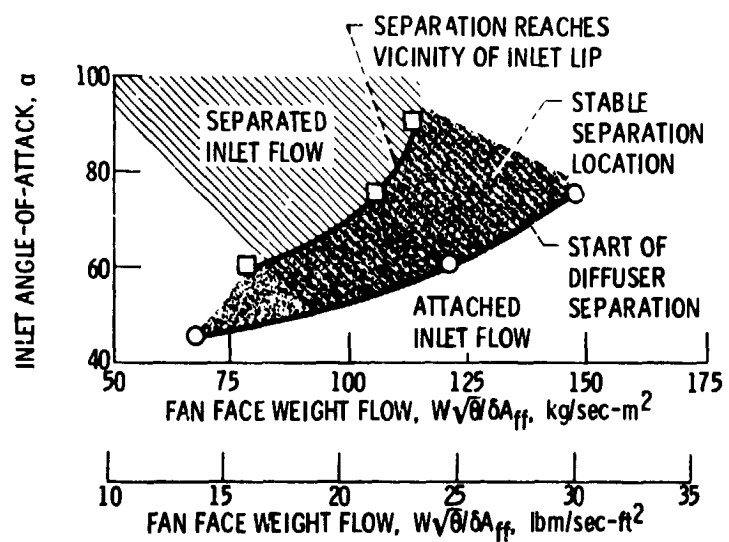


Figure 10. - Tilt nacelle inlet separation boundaries for $V_{\infty} = 54$ m/sec (105 knots).

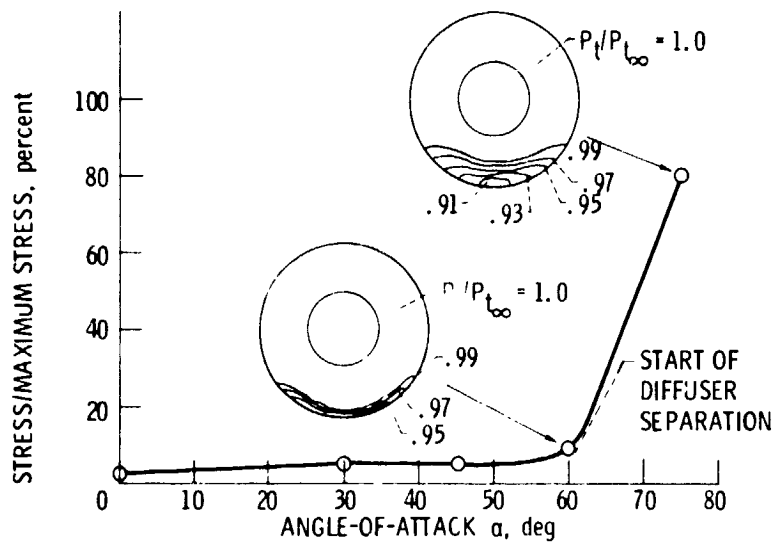


Figure 11. - Variation of E05 stress level with angle-of-attack, $V_\infty = 54$ m/sec (105 knots).

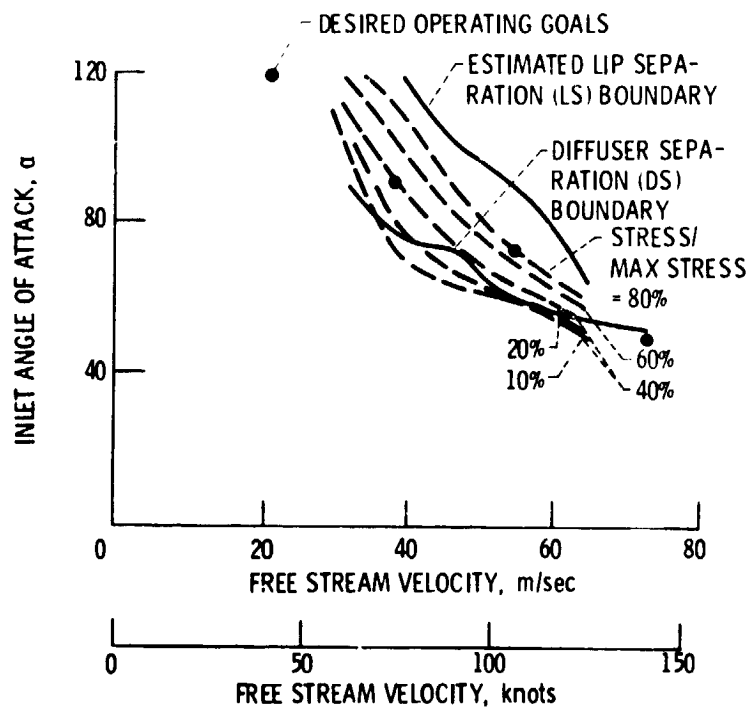


Figure 12. - Comparison of tilt nacelle inlet low speed design goals with expected engine order five (E05) stress levels.

ORIGINAL PAGE IS
OF POOR QUALITY